IEEE Access
Multidisciplinary : Rapid Review : Open Access Journal

Received February 4, 2019, accepted February 24, 2019, date of publication March 4, 2019, date of current version March 29, 2019.

Digital Object Identifier 10.1109/ACCESS.2019.2902852

Compact and Wideband General Coupled-Line Ring Hybrids (GCRHs) for Arbitrary Circumferences and Arbitrary Power-Division Ratios

HEE-RAN AHN, (Senior Member, IEEE), AND MANOS M. TENTZERIS, (Fellow, IEEE)
School of Electrical and Computer Engineering, Georgia Institute of Technology, Atlanta, GA 30332, USA

Corresponding author: Hee-Ran Ahn (hranahn@gmail.com)

This work was supported by the NSF.

ABSTRACT Coupled-line ring hybrids (CRHs) are presented for arbitrary circumferences and for arbitrary power-division ratios. They each consist of three single transmission-line sections and a set of coupled transmission-line sections with or without two identical capacitances and contain most properties of the conventional ring hybrids. Therefore, they may be called general CRHs and can be designed for the frequency performance better than that of any other conventional one. By adopting the coupled-line sections, the 180° phase shift can be guaranteed, regardless of fabrication technologies, but three or four unknown variables more should be considered additionally, which results in a complicated derivation process. To make it simpler, two conditions of $S_{11}^{e} = S_{22}^{o}$ and $S_{22}^{e} = S_{11}^{o}$, where S_{11} and S_{22} are scattering parameters, and the superscripts of e and o are meant as even- and odd-mode excitations, respectively, are newly employed. To verify the suggested theory, two prototypes were tested for the power-division ratios of 0 and −5 dB without and with capacitances, respectively. The measured results are in good agreement with the predicted ones, and the measured bandwidths with 15-dB return loss are 82.9 % and 97.65 % for the power-division ratios of 0 and −5 dB, respectively.

INDEX TERMS General coupled-line ring hybrids (GCRHs), coupled-line ring hybrids (CRHs), wide-band ring hybrids, arbitrary circumferences, arbitrary power-division ratios, rat-race couplers, bandwidth enhancement method, coupled transmission-line sections.

I. INTRODUCTION

The ring hybrids (RHs) [1]–[17] originate from Tyrrel [1] in 1947 and have been used for various applications such as phase shifters, antenna arrays, mixers and balancing amplifiers. The typical RH consists of three 90° and one 270° transmission-line sections (TLs), and its bandwidth is as small as 10 %, because the bandwidth of the 270° TL is small. To increase the bandwidths, March [2] replaces the 270° TL with a set of 90° coupled transmission-line sections (CPL), two ports of which are short-circuited in a diagonal direction. However, the performance of the RH is possible only with −3 dB coupling coefficient, and the design formulas are applicable only for equal power divisions. To overcome the restrictions, design formulas, which can be applied for any coupling coefficient, are derived for the RHs with equal power divisions [6], [7] and with arbitrary power-division ratios [8], [9], and those structures have been called coupled-line ring hybrids (CRHs) [6]–[9]. However, all TLs and CPLs of the CRHs should be 90° long.

In this paper, to reduce the size of the CRHs and to increase bandwidths and design flexibilities, deign methods are suggested for arbitrary circumferences and for arbitrary power-division ratios. Since the CRHs to be discussed in this paper contain all the properties of the conventional CRHs and RHs, they may be named general coupled-line RHs (GCRHs).

For the arbitrary circumferences, several conventional ways [10]–[14] exist. However, they are not desirable [10], [11], not valid for arbitrary power-division ratios [12], [13], or not for the wideband performance [14]. In [10], only approximate solutions are available for the arbitrary termination impedances and for the arbitrary

The associate editor coordinating the review of this manuscript and approving it for publication was Kuang Zhang.

power-division ratios. In [11], the 180° phase shift can function only at 0 GHz [11, Fig. 8(c)]. In [14], a TL is simply extended to have 180° phase difference, leading to small bandwidths. In [12] and [13], the RH properties are demonstrated for the equal power divisions, but the design formulas are derived under the assumption of ideal 180° phase shift which must be realized with uniplanar structures where wires are soldered to connect two TLs. However, the wires could work as very high values of inductance or high impedance TLs which causes the frequency performance to deteriorate.

On the contrary, the CPL to be discussed in this paper gives the 180° phase shift without any restriction on the fabrication technology, which is a big advantage over the conventional methods together with more design flexibility. The GCRHs suggested in this paper each consist of three TLs and one CPL with or without two identical capacitances, and all TLs including CPL are of arbitrary electrical lengths. Two of three TLs should be identical, and the rest one and the CPL are different from each other. Therefore the derivation process for the design formulas could be very complicated, even though even- and odd-mode excitation analyses can be possible. To make it simpler, two conditions of $S_{11}^e = S_{22}^o$ and $S_{22}^e = S_{11}^o$, where S_{11} and S_{22} are scattering parameters, and the superscripts of e and o are meant as even- and odd-mode excitations respectively, are applied for the CPLs reversely. The two key points to be solved in this paper are how to get the three TLs with arbitrary lengths, and how to get the CPLs with arbitrary lengths, as well.

Depending on with or without capacitances, the design formulas for the CPLs are different, and the exact design formulas for the CRHs without the capacitance may be tried for the first time in this paper, because they are possible only with the correct even- and odd-mode impedances in [6, eq. (9)] and [7, eq.(11)] for the CPLs. The CPLs with the capacitances are discussed in [7, Fig. 6] and [9, Fig. 2]. The applications are, however, limited to 90° CPLs for equal power divisions [7] or arbitrary power-division ratios [9], and the design formulas to be derived in this paper are different from those in [7] and [9]. Depending on with or without the capacitances, two types of GCRHs are available, and both types of GCRHs have never been suggested before for the exact solutions. To verify the design methods, two prototypes with the power-division ratios of 0 and −5 dB are exemplified and measured at the design frequency of 2 GHz.

II. GENERAL COUPLED-LINE RING HYBRIDS

The GCRH terminated in equal admittances of $Y_0 = Z_0^{-1}$ is depicted in Fig. 1(a) where it consists of three TLs and one CPL with two identical capacitances C_{ap}s. The characteristic admittances and the electrical lengths of the TLs are ($Y_1 = Z_1^{-1}$, Θ_1) and ($Y_2 = Z_2^{-1}$, Θ_2), and the even- and odd-mode admittances and the electrical length of the CPL are $Y_{0e} = Z_{0e}^{-1}$, $Y_{0o} = Z_{0o}^{-1}$ and Θ_3, respectively. The CPL and its equivalent circuit [6, Fig. 7], [18, Fig. 1] are depicted in Fig. 1(b), consisting of two identical short stubs

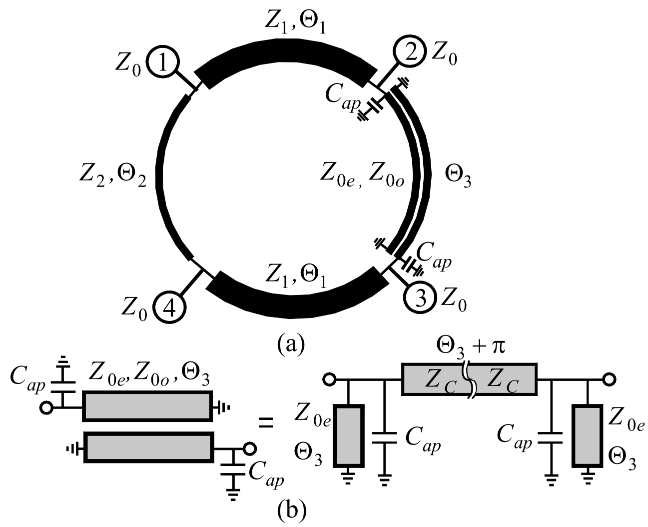

FIGURE 1. (a) GCRH topology. (b) Equivalent circuit of the CPL between ports ② and ③.

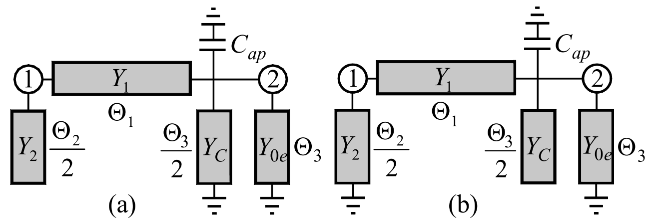

FIGURE 2. (a) Even-mode equivalent circuit. (b) Odd-mode equivalent circuit.

with the characteristic admittance of Y_{0e} and the electrical length of Θ_3 and one TL with the characteristic admittance of $Y_C = Z_C^{-1}$ and the electrical length of $\Theta_3+\pi$.

The even- and odd-mode equivalent circuits of the GCRH are illustrated in Fig. 2(a) and (b), respectively, and the even- and odd-mode admittances are given as

$$\begin{bmatrix} Y_{11}^e & Y_{12}^e \\ Y_{21}^e & Y_{22}^e \end{bmatrix} = \begin{bmatrix} -jY_1\cot\Theta_1 + jY_2\tan\frac{\Theta_2}{2} & jY_1\csc\Theta_1 \\ jY_1\csc\Theta_1 & -jY_1\cot\Theta_1 - jY_{ke} \end{bmatrix} \quad (1a)$$

$$\begin{bmatrix} Y_{11}^o & Y_{12}^o \\ Y_{21}^o & Y_{22}^o \end{bmatrix} = \begin{bmatrix} -jY_1\cot\Theta_1 - jY_2\cot\frac{\Theta_2}{2} & jY_1\csc\Theta_1 \\ jY_1\csc\Theta_1 & -jY_1\cot\Theta_1 + jY_{ko} \end{bmatrix} \quad (1b)$$

where the superscripts of "e" and "o" are meant as the even- and odd-mode excitations, and Y_{ke} and Y_{ko} are

$$Y_{ke} = Y_{0e}\cot\Theta_3 - \omega C_{ap} + Y_C\cot\frac{\Theta_3}{2} \quad (2a)$$

$$Y_{ko} = -Y_{0e}\cot\Theta_3 + \omega C_{ap} + Y_C\tan\frac{\Theta_3}{2} \quad (2b)$$

where

$$Y_C = \frac{Y_{0o} - Y_{0e}}{2} \quad (2c)$$

The even- and odd-mode scattering parameters of $S_{ij}^{e,o}$ are, referring to [17, Table 2.2], formulated as

$$S_{11}^{e,o} = -\frac{\left(Y_{11}^{e,o} - Y_0\right)\left(Y_{22}^{e,o} + Y_0\right) - Y_{12}^{e,o}Y_{21}^{e,o}}{\Delta_y^{e,o}} \tag{3a}$$

$$S_{12}^{e,o} = S_{21}^{e,o} = -\frac{2Y_{12}^{e,o}Y_0}{\Delta_y^{e,o}} = -\frac{2Y_{21}^{e,o}Y_0}{\Delta_y^{e,o}} \tag{3b}$$

$$S_{22}^{e,o} = -\frac{\left(Y_{11}^{e,o} + Y_0\right)\left(Y_{22}^{e,o} - Y_0\right) - Y_{12}^{e,o}Y_{21}^{e,o}}{\Delta_y^{e,o}}, \tag{3c}$$

where $\Delta_y^{e,o} = \left(Y_{11}^{e,o} + Y_0\right)\left(Y_{22}^{e,o} + Y_0\right) - Y_{12}^{e,o}Y_{21}^{e,o}$.

In principle, the admittance parameters in (1) should be substituted into (3) for the design formulas. However, the unknown variables are Y_1, Y_2, Θ_1, Θ_2, Y_{0e}, Y_{0o} and Θ_3, too many for the available two conditions (power divisions and perfect matching) to get the correct solutions. It is therefore necessary to reduce number of variables, and to think reversely is one of ways to reach the correct solutions easily. For the RH properties, $S_{11}^e = S_{22}^o$ and $S_{22}^e = S_{11}^o$ should be, from which the following two conditions are obtained.

$$Y_{11}^e = Y_{22}^o \quad \text{and} \quad Y_{22}^e = Y_{11}^o \tag{4}$$

Applying the conditions in (4) to (1) and (2) gives two relations as

$$Y_{ke} = Y_2 \cot\frac{\Theta_2}{2}, \tag{5a}$$

$$Y_{ko} = Y_2 \tan\frac{\Theta_2}{2} \tag{5b}$$

Substituting (1) and (2) with (5) into (3), scattering parameters of the even- and odd-mode equivalent circuits in Fig. 2(a) and (b) are derived as

$$S_{11}^e = S_{22}^o = -\frac{A + jB}{\Delta_y} \tag{6a}$$

$$S_{21}^e = S_{21}^o = -\frac{j2Y_1Y_0\csc\Theta_1}{\Delta_y} \tag{6b}$$

$$S_{22}^e = S_{11}^o = -\frac{A - jB}{\Delta_y} \tag{6c}$$

where $\Delta_y = \Delta_y^e = \Delta_y^o$

$$A = Y_1^2 - 2Y_1Y_2\cot\Theta_1\cot\Theta_2 + Y_2^2 - Y_0^2 \tag{6d}$$

$$B = 2Y_2Y_0\csc\Theta_2 \tag{6e}$$

The final scattering parameters of the GCRH in Fig. 1(a) are

$$S_{11} = S_{22} = \frac{S_{11}^e + S_{11}^o}{2} = \frac{S_{22}^e + S_{22}^o}{2} = -\frac{A}{\Delta_y} \tag{7a}$$

$$S_{21} = S_{43} = \frac{S_{21}^e + S_{21}^o}{2} = -j\frac{2Y_1Y_0\csc\Theta_1}{\Delta_y} \tag{7b}$$

$$S_{31} = S_{42} = \frac{S_{21}^e - S_{21}^o}{2} = 0 \tag{7c}$$

$$S_{41} = \frac{S_{11}^e - S_{11}^o}{2} = -j\frac{B}{\Delta_y} \tag{7d}$$

$$S_{23} = \frac{S_{22}^e - S_{22}^o}{2} = j\frac{B}{\Delta_y} \tag{7e}$$

The ratios of S_{21} to S_{41} and S_{43} to S_{23} are expressed to give

$$\frac{S_{21}}{S_{41}} = -\frac{S_{43}}{S_{23}} = \frac{Y_1\csc\Theta_1}{Y_2\csc\Theta_2}. \tag{8}$$

The power-division ratio of k^2 is therefore simplified as

$$k = \left|\frac{S_{21}}{S_{41}}\right| = \left|\frac{S_{43}}{S_{23}}\right| = \frac{Z_2\sin\Theta_2}{Z_1\sin\Theta_1}, \tag{9}$$

where $\Theta_1 \neq 0°$ and $\Theta_2 \neq 0°$. Using the perfect matching condition ($7a$) and the power- division ratio of k^2 in (9), the design formulas for $Z_1 = Y_1^{-1}$ and $Z_2 = Y_2^{-1}$ are derived as

$$Z_1 = \frac{\Psi}{k sin\Theta_1}Z_0, \quad Z_2 = \frac{\Psi}{sin\Theta_2}Z_0 \tag{10}$$

where $\Psi = \sqrt{\left(k^2+1\right) - \left(k cos\Theta_1 + cos\Theta_2\right)^2}$

When $k^2 = 1$ and $\Theta_1 = \Theta_2 = 90°$ in (10), $Z_1 = Z_2 = \sqrt{2}\,Z_0$ is obtained, which is the same as that of the conventional one [1], [7]. When $\Theta_1 = \Theta_2 = 90°$ in (10), the design formulas are the same as those in [8] and [17]. When $k^2 = 1$ and $\Theta_1 = \Theta_2, k^2 = 1$ and $\Theta_1 \neq \Theta_2$ or arbitrary values of k^2, Θ_1 and Θ_2, they are the same as those in [11]–[13] and [19].

To have real values of Z_1 and Z_2, regardless of k, the following relation holds;

$$sin^2\Theta_1 + sin^2\Theta_2 > 1 \tag{11}$$

In addition, another condition for Θ_1 and Θ_2 that the values of Z_1 and Z_2 are less than those with $\Theta_1 = \Theta_2 = 90°$ in ($7a$) should be satisfied as

$$\cot\Theta_1\cot\Theta_2 > 0 \tag{12}$$

The condition in (12) implies $0 < \Theta_1, \Theta_2 \leq 90°$ or $90^o < \Theta_1, \Theta_2 < 180°$, but only the case of shorter lengths will be treated in this paper. The design formulas in (10) can be applied for the single TLs only in Fig. 1, and those for the CPLs should be solved using equations (5) where two cases are available depending on $\omega C_{ap} = 0$ or $\omega C_{ap} \neq 0$.

A. CPLs WITH $C_{ap} = 0$

In this case with $\omega C_{ap} = 0$, three design formulas can be derived by $Y_{ke} \cdot Y_{ko}$, $Y_{ke} + Y_{ko}$ and $Y_{ke} - Y_{ko}$ in (2) and (5) to give

$$Y_2^2 = Y_C^2 - Y_{0e}Y_{0o}\cot^2\Theta_3 \tag{13a}$$

$$Y_2\csc\Theta_2 = Y_C\csc\Theta_3 \tag{13b}$$

$$Y_2\cot\Theta_2 = \frac{Y_{0o} + Y_{0e}}{2}\cot\Theta_3 \tag{13c}$$

Based on the characteristic admittance of Y_C in (2c) and the coupling coefficient C, the even- and odd-mode admittances of Y_{0e} and Y_{0o} can be derived as

$$Y_{0e} = Y_C\frac{1-C}{C}, \quad Y_{0o} = Y_C\frac{1+C}{C} \tag{14}$$

where

$$C = \frac{Y_{0o} - Y_{0e}}{Y_{0o} + Y_{0e}} \tag{14a}$$

From the design formulas in (13), it can be known that the designs of the CPLs are determined by the values of $Y_2 = Z_2^{-1}$ and Θ_2, which can be obtained from (10). From (13), the electrical length of Θ_3 and C are expressed with Y_2, Θ_2 and Y_C as

$$C = \frac{\sqrt{(Y_2 \csc\Theta_2)^2 - Y_C^2}}{Y_2 \cot\Theta_2} \tag{15a}$$

$$\Theta_3 = sin^{-1}\left(\frac{Y_C}{Y_2}\sin\Theta_2\right) \tag{15b}$$

$$\cot^2\Theta_3 = \frac{Y_C^2 - Y_2^2}{Y_{0e}Y_{0o}} \tag{15c}$$

Applying two conditions of $\sin\Theta_3 \leq 1$ in (15b) and $\cot^2\Theta_3 > 0$ in (15c) gives the boundary condition for $Z_C = Y_C^{-1}$ as

$$Z_2 > Z_C \geq Z_2 \sin\Theta_2 \tag{16}$$

B. CPLs WITH $C_{ap} \neq 0$

When $C_{ap} \neq 0$, the design formulas for the CPLs can be derived from (2) and (5) as

$$Y_C = \frac{Y_2 csc\Theta_2}{csc\Theta_3} \tag{17a}$$

$$\omega C_{ap} = \frac{Y_C}{C}\cot\Theta_3 - Y_2 \cot\Theta_2 \tag{17b}$$

Similarly, with the available Z_2 and Θ_2 from (10), the CPLs with $C_{\text{ap}} \neq 0$ can be designed. Quite different from the CPLs with $C_{\text{ap}} = 0$, more design flexibility is possible, because of one free variable of C_{ap} more. Based on arbitrarily determined Θ_3 in (17a), the value of Y_C can be calculated. If coupling coefficient of C in (17b) is chosen arbitrarily, the value of C_{ap} can be calculated at a given design frequency. There is, in principle, no restriction on Θ_3 but the optimal value is around Θ_2.

The equations in (6b) and (7b) give $S_{12}^e = S_{12}^o = 2S_{21} = 2S_{43}$ which means, if the power divisions are guaranteed, the isolation is also guaranteed. Therefore, hereafter the isolation performance does not need to be treated.

III. DESIGN EXAMPLES FOR $k^2 = 0$ AND -5 dB.

For the GCRHs with $C_{ap} = 0$ or $C_{ap} \neq 0$, the design process is illustrated in Fig. 3. With the desired power-division ratio of k^2, the two electrical lengths of Θ_1 and Θ_2 are determined arbitrarily, based on (11) and (12). Then, the two characteristic impedances of Z_1 and Z_2 can be calculated using (10) as shown in Fig. 3(a). Now, the CPLs are ready to be designed with the available Z_2 and Θ_2. For the designs of the CPLs with $C_{\text{ap}} = 0$ in Fig. 3(b), the first thing is to determine Y_C arbitrarily, based on (16). Then, the coupling coefficient of C and the electrical length of Θ_3 are able to be calculated using (15a) and (15b). Based on C, the final values of Y_{0e}

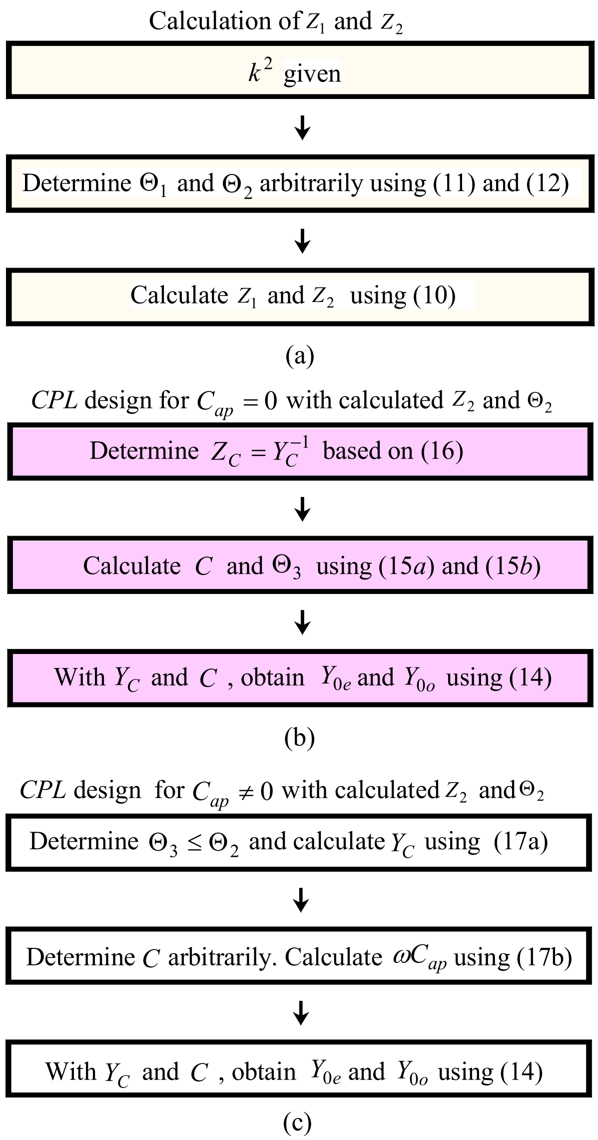

FIGURE 3. Design process for GCRHs. (a) Calculation of Z_1 and Z_2. (b) CPL design for $C_{ap} = 0$. (c) CPL design for $C_{ap} \neq 0$.

and Y_{0o} are obtained from (14). Then, the design of the CPLs with $C_{\text{ap}} = 0$ is completed. The designs are not restricted on the coupling coefficients of C in (15a), and therefore any coupling coefficient can be selected by choosing appropriate values of Y_C.

For CPLs of GCRHs with $C_{\text{ap}} \neq 0$ in Fig. 3(c), there is no restriction, and therefore the designs are easier than those for GCRHs with $C_{\text{ap}} = 0$. First of all, determine Θ_3 around Θ_2 and then calculate Y_C using (17a). With arbitrarily selected coupling coefficients of C depending on the fabrication situation, calculate the value of C_{ap} with the calculated value of Y_C and the predetermined value of C. With Y_C and C, the values of Y_{0e} and Y_{0o} are finally calculated based on (14).

Depending on the power-division ratios of $k^2 = 0$ and -5 dB, the designs of GCRHs will be discussed in more detail. Hereafter, the GCRHs will be meant as those

TABLE 1. Design parameters of GCRHs for $k^2 = 0$ dB.

$Z_1 = Z_2 = 65.86\ \Omega$ and $\Theta_1 = \Theta_2 = 70^\circ$				
Z_C	Z_{0e}	Z_{0o}	Θ_3	C(dB)
62.6 Ω	49.1 Ω	19.11 Ω	81.4°	-7.14
63.0 Ω	76.0 Ω	22.27 Ω	79.2°	-5.24
64.0 Ω	186.7Ω	27.32 Ω	75.2°	-2.56
65.0 Ω	546.7 Ω	30.68 Ω	72.2°	-0.98

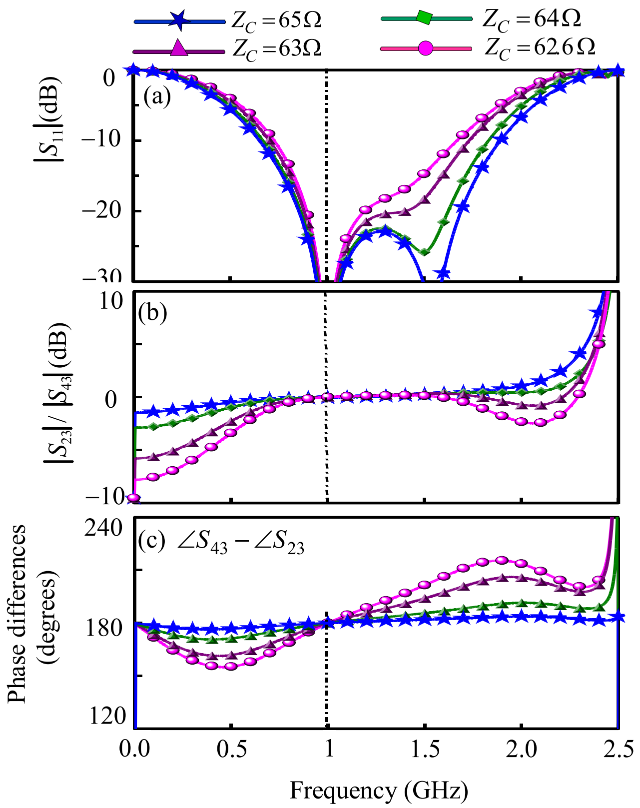

FIGURE 4. Frequency responses of GCRHs with $C_{ap} = 0$ for $k^2 = 0$ dB. (a) $|S_{11}|$. (b) Power-division ratios of $|S_{23}|\,/\,|S_{43}|$. (c) Out-of-phase responses of $\angle S_{43} - \angle S_{23}$.

without C_{ap}, while those with C_{ap}s named GCRHCs to distinguish from each other.

A. GCRHs FOR $k^2 = 0$ dB

When $k^2 = 0$ dB, many design sets are possible, and one case of $\Theta_1 = \Theta_2 = 70^\circ$ is selected, leading to $Z_1 = Z_2 = 65.86\ \Omega$ from (10). Referring to the design formulas in (16), the values for Z_C should be $61.89\ \Omega \le Z_C < 65.86\ \Omega$, meaning that the design parameters of the CPLs are determined by the values of Z_C. The design parameters for Z_{0e}, Z_{0o} and Θ_3 are listed in Table 1 by varying the values of Z_C. The design parameters in Table 1 find that the characteristic impedances of Z_C and the coupling coefficients of C are inversely proportional to the electrical lengths of Θ_3. Based on the design parameters in Table I, the frequency responses of the GCRHs were simulated at the design frequency of 1 GHz and plotted in Fig. 4 where the responses of $|S_{11}|$ are in Fig. 4(a), power-division ratios of $|S_{23}|$ to $|S_{43}|$ ($|S_{23}|\,/\,|S_{43}|$) in Fig. 4(b) and phase differences of $\angle S_{43} - \angle S_{23}$ in Fig. 4(c).

TABLE 2. For $k^2 = 0$ dB, compared design parameters between GCRH and conventional ones [1], [6].

	$Z_1 = Z_2$	$Z_{0e}(\Omega), Z_{0o}(\Omega)$	Total Lengths
GCRH	65.86 Ω	49.08, 19.11	291.36°
CRH[6]	70.71 Ω	55.46, 21.59	360°
[1]	70.71 Ω		540°

The bandwidth with the 15-dB return loss is about 98 % (0.76-1.75 GHz) when $Z_C = 65\ \Omega$. Those with $Z_C = 64$, 63 and 62.6 Ω are 93.5 % (0.72-1.785 GHz), 77.5 % (0.825-1.6 GHz) and 67 % (0.83-1.5 GHz), respectively. As demonstrated in Fig. 4(a), the bandwidths of the GCRHs are proportional to the coupling coefficients of C. The power-division ratios are all 0 dB at 1 GHz, and wideband characteristics are shown in Fig. 4(b). The phase differences of $\angle S_{43} - \angle S_{23}$ in Fig. 4(c) are all 180° at 1 GHz, and the bandwidths are wider with Z_C closer to Z_2.

The two cases with $Z_C = 62.6$ and 63 Ω in Table 1 can be fabricated in planar structures without any problem, and the responses with $Z_C = 62.6\ \Omega$ are worse than those with $Z_C = 63\ \Omega$. The worse frequency responses with $Z_C = 62.6\ \Omega$ are compared to those with the conventional ones [1], [6]. For the CRH in [6], the characteristic impedances of Z_1 and Z_2 are 70.71 Ω, and its corresponding even- and odd-mode impedances with the same coupling coefficient of −7.14 dB are 55.46 and 21.59 Ω, respectivly. For the conventional RH in [1], the characteristic impedances of Z_1 and Z_2 are 70.71 Ω, and one TL is extended by 180° long. The total TLs of the GCRH is 291.36° long, whereas those of the CRH in [6] and the typical conventional one in [1] are 360° and 540° long, respectively. The design parameters and total TL lengths are listed in Table II, based on which frequency responses are compared in Fig. 5 where matching responses of $|S_{11}|$ are in Fig. 5(a), the power-division ratios of $|S_{41}|$ to $|S_{21}|$ in Fig. 5(b) and out-of-phase responses of $\angle S_{43} - \angle S_{23}$ in Fig. 5(c).

In Fig. 5(a), the 15-dB return loss bandwidth of the GCRH is 67 % (0.83-1.4 GHz), while those of CRH and conventional one are 54 % (0.73-1.27GHz) and 40 % (0.8-1.2 GHz), respectively. For the power-division ratios of $|S_{41}|\,/\,|S_{21}|$ in Fig. 5(b), the bandwidth with ± 1 dB of the GCRH is 75 % (0.75-1.5 GHz), those of CRH and the conventional ones are 70 % (0.65-1.35 GHz) and 31.1 % (0.84-1.15 GHz), respectively. For the out-of-phase responses in Fig. 5(c), the bandwidth with the phase difference of 150° -200° of the GCRH is 168 % (0-1.68 GHz), while those of the other two are 149.9 % (0-1.499 GHz) and 61 % (0.72-1.33 GHz). The compared properties are collected in Table 3 where it can be easily observed that in terms of matching property, power-division ratio and out-of-phase responses, the GCRH is the best, even with the smallest size.

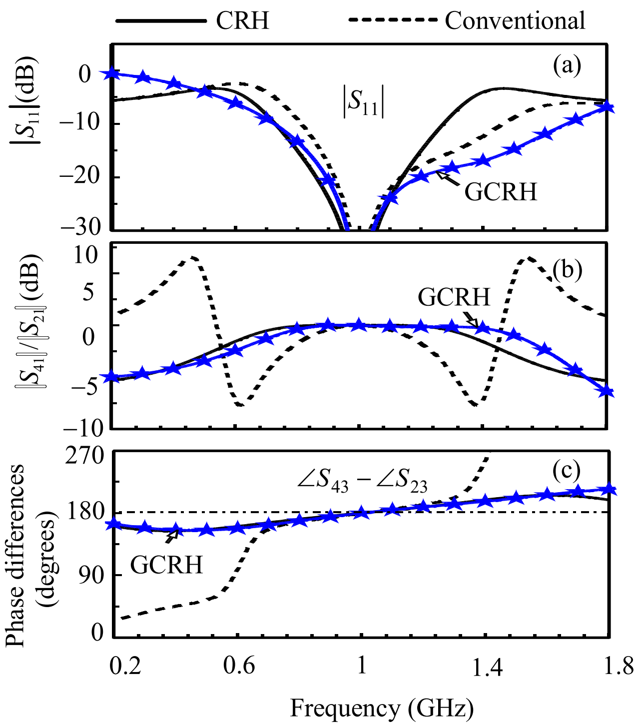

FIGURE 5. Compared frequency responses for $k^2 = 0$ dB. (a) $|S_{11}|$. (b) Power-division ratios of $|S_{41}| / |S_{21}|$. (c) Out-of-phase responses of $\angle S_{43} - \angle S_{23}$.

TABLE 3. Compared frequency performance for $k^2 = 0$ dB.

	BW of $\|S_{11}\|$	BW of $\|S_{41}\|/\|S_{21}\|$	BW of $\|\angle S_{23} - \angle S_{43}\|$
GCRH	67.0 %	75 %	168.0 %
CRH [6]	54.0 %	70 %	149.9 %
[1]	40.0 %	31 %	61.0%

TABLE 4. Design parameters of GCRHCs for $k^2 = -5$ dB.

$Z_1 = 98.8\ \Omega,\ Z_2 = 55.6\ \Omega,\ \Theta_1 = \Theta_2 = 75^{\circ}$.				
$C(dB)$	Θ_3	$Z_{0e}(\Omega)$	$Z_{0o}(\Omega)$	C_{ap}(pF)
-3	77°.	133.55	22.84	0.17
-5	75°	71.41	20.00	0.60
-7	72°	45.57	17.43	1.28
-9	70°	31.42	14.96	2.09
-11	68°	22.72	12.73	3.17

B. GCRHCs FOR $k^2 = -5$ dB

When $k^2 = -5$ dB, many designs are also possible, and one of them is when $\Theta_1 = \Theta_2 = 75^{\circ}$. In this case, $Z_1 = 98.83\ \Omega$ and $Z_2 = 55.58\ \Omega$ can be calculated from (10). For the designs of the CPLs, with Θ_3 around 75° and the coupling coefficients of C varying, the even- and odd-mode impedances of Z_{0e} and Z_{0o} and the capacitance values of C_{ap} are, based on (17) and (14), calculated in Table 4 where the values of C_{ap} are those at 1 GHz. When $C = -3$ dB, the values of Z_{0e} and Z_{0o} are 133.55 and 22.84 Ω, respectively, and the required capacitance of C_{ap} is 0.17 pF at 1 GHz. As the coupling coefficient goes lower in Table 4, the values of Z_{0e} and Z_{0o} become smaller, while the capacitance values of C_{ap} are higher.

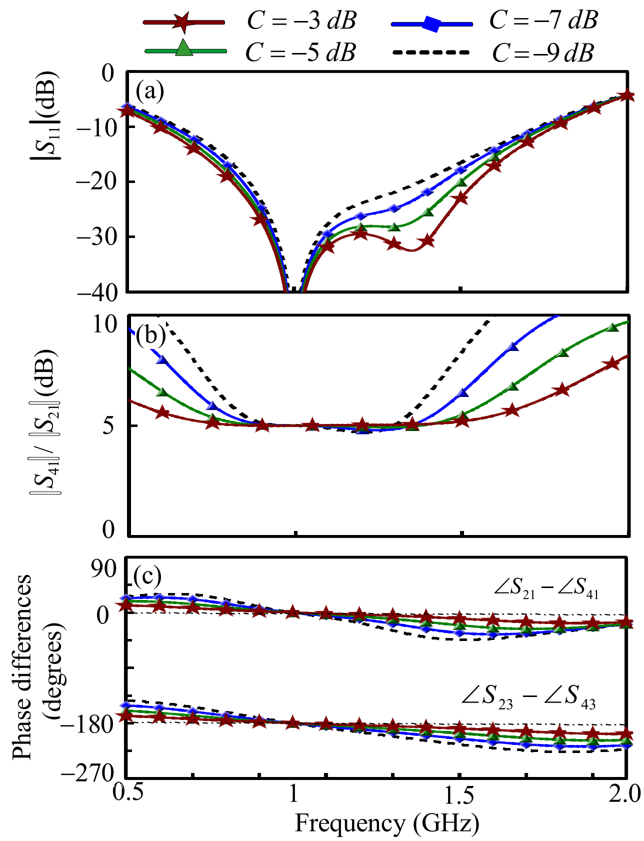

FIGURE 6. Frequency responses of GCRHCs for $k^2 = -5$ dB. (a) $|S_{11}|$. (b) Power-division ratios of $|S_{41}| / |S_{21}|$. (c) In- and out-of-phase responses.

Based on the design parameters in Table 4, the frequency responses of the four cases of $C = -3, -5, -7$ and -9 dB were simulated at the design frequency of 1 GHz, and the frequency responses are plotted in Fig. 6 where those of $|S_{11}|$ are in Fig. 6(a), power-division ratios of $|S_{41}|$ to $|S_{21}|$ in Fig. 6(b), and in- and out-of-phase differences in Fig. 6(c). The 15-dB return loss bandwidth of $|S_{11}|$ with $C = -3$ dB is 93 % (0.71-1.64 GHz), and those with $C = -5$ and -7 dB are 87 % (0.74-1.61 GHz) and 80 % (0.77-1.57 GHz), respectively. All the cases are perfectly matched at 1 GHz, perfect power-division ratios of −5 dB, perfect 180° out-of-phase and perfect 0° in–phase responses are achieved at 1 GHz, as well.

C. BANDWIDTHS AND HIGHEST POWER-DIVISION RATIO

Referring to frequency responses in Fig. 4, higher values of Z_C give wider bandwidths, and the values of Z_C are proportional to the coupling coefficients in Table 1. Therefore the bandwidths are proportional to the coupling coefficients for the GCRHs. For GCRHCs in Fig. 6, the bandwidths

TABLE 5. Design and fabrication parameters of prototype I for $k^2 = 0$ dB.

$Z_1 = Z_2 = 65.86\ \Omega$, $\Theta_1 = \Theta_2 = 70^\circ$
$w = 1.19$ mm, $\ell = 19$ mm
$Z_{0e} = 75.99\ \Omega$, $Z_{0o} = 22.27\ \Omega$, $\Theta_3 = 79.23^\circ$
$C_1 =$ -5.24 dB $\rightarrow$ $w_c = 1.30$ mm, $s_c = 0.24$ mm, $w_v = 0.33$ mm, $\ell_c = 21.3$ mm

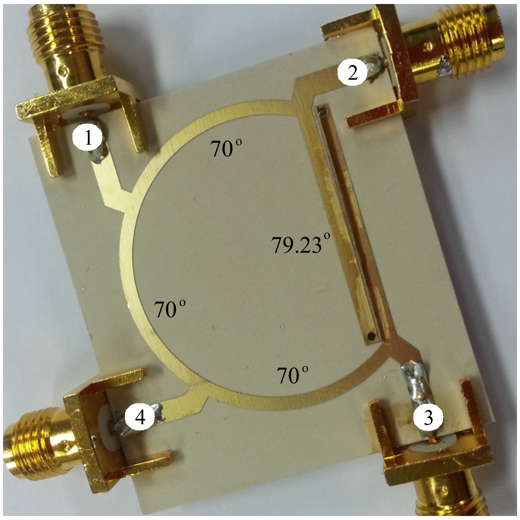

FIGURE 7. Fabricated prototype I (GCRH) for $k^2 = 0$ dB.

are proportional to the coupling coefficients, as well. However, the cases with $Z_C = 64$ and $65\ \Omega$ in Table 1 are unfeasible, because of unrealizable high values of even-mode impedances.

Since two variables of Θ_1 and Θ_2 can control the power-division ratios of k in (9), the GCRHs have an advantage in terms of high power-division ratios. For example of $k^2 = 15$ dB, $\Theta_1 = 30^\circ$ and $\Theta_2 = 90^\circ$ satisfying (11) gives $Z_1 = 53\ \Omega$ and $Z_2 = 149.2\ \Omega$ in (10). If Θ_3 and the coupling coefficient are selected as 85° and $C = -6.8$ dB respectively for the GCRHC, even-, odd-mode impedances and the capacitance value can be calculated as $Z_{0e} = 126\ \Omega$, $Z_{0o} = 47\ \Omega$ and 0.2 pF at 1 GHz, respectively. Since all the design parameters can be feasible with the microstrip format, the 15-dB power-division ratio can be achieved.

IV. MEASUREMENTS

For the proof-of-concept demonstration, two prototypes for $k^2 = 0$ dB and -5 dB were designed at 2 GHz and fabricated on an available substrate (RO3003, $\varepsilon_r = 3$, $H = 0.75$ mm).

A. PROTOTYPE I FOR $k^2 = 0$ dB

For the prototype I, the GCRH configuration was used, and the design parameters with $Z_C = 63\ \Omega$ in Table 1 were applied. The design and fabrication parameters for the prototype I are collected in Table 5.

In Table 5, the physical dimensions of width w and length l of the single TLs are $w = 1.19$ mm and l=19 mm at 2 GHz.

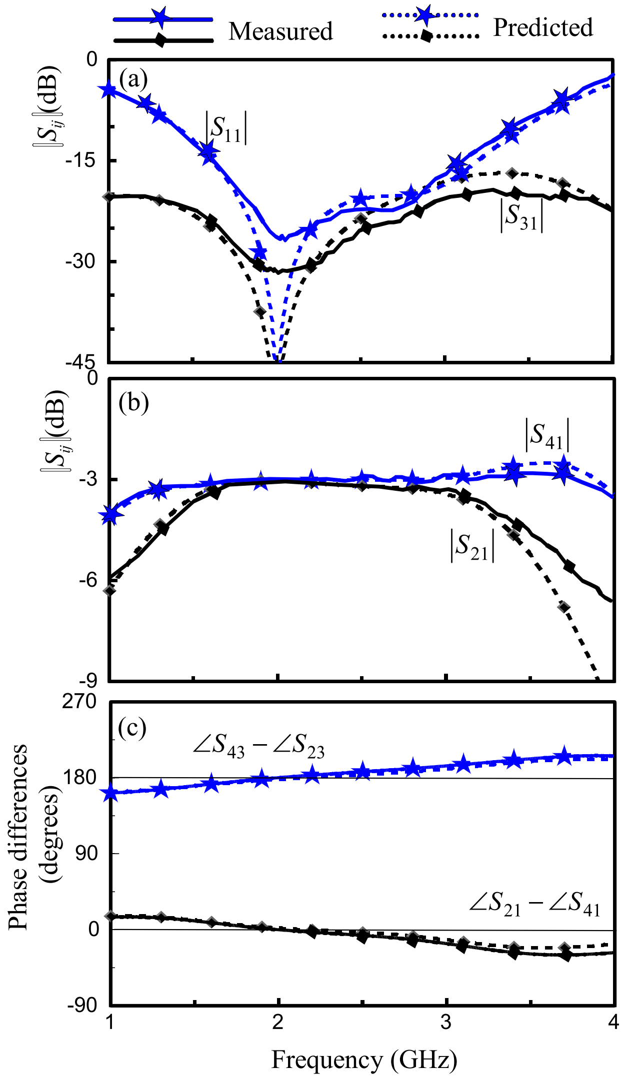

FIGURE 8. Measured and predicted frequency responses of prototype I (GCRH) for $k^2 = 0$ dB. (a) $|S_{11}|$ (matching) and $|S_{31}|$ (isolation). (b) Power divisions of $|S_{21}|$ and $|S_{41}|$. (c) In- and out-of-phase responses.

The coupling coefficient of the CPL is $C = -5.24$ dB, which does not seem to be possible on the given substrate with a microstrip planar structure. Any 3D structure in [6, Fig. 8] and [20, Fig. 18] is, therefore, needed. For a given substrate, first consider $Z_{0e} = 75.99\ \Omega$ and $Z_{0o} = 44.3\ \Omega$, whose physical dimensions are width $w_c = 1.30$ mm and gap space $s_c = 0.24$ mm. To achieve the required value of $Z_{0o} = 22.27\ \Omega$, the impedance produced by the vertical conductor in [6, Fig. 8(b)] and [20, Fig. 18] should be $Z_v = 44.78\ \Omega$. The physical dimension of vertical width w_v for Z_v can be obtained by one of 3D full wave simulators such as Ansys HFSS in a similar way in [20, Fig. 19]. The fabricated prototype I is demonstrated in Fig. 7.

The frequency responses measured and predicted are compared in Fig. 8 where matching at port ① and isolation responses are in Fig. 8(a), the power divisions in Fig. 8(b) and phase responses in Fig. 8(c). The measured $|S_{11}|$ and $|S_{31}|$ in Fig. 8(a) are -27.38 and -32.52 dB at 2 GHz, respectively.

TABLE 6. Design and fabrication parameters of prototype II (GCRHC) for $k^2 = -5$ dB.

$Z_1 = 98.83\ \Omega$, $Z_2 = 55.58\ \Omega$, $\Theta_1 = \Theta_2 = \Theta_3 = 75°$.
$w_1 = 0.51$ mm, $\ell_1 = 20.89$ mm $w_2 = 1.61$ mm, $\ell_2 = 20.17$ mm
$Z_{0e} = 71.41\ \Omega$, $Z_{0o} = 20\ \Omega$, $C_{ap} = 0.3$ pF at 2 GHz.
$C_2 = $ -5.0 dB $\rightarrow w_c = 1.45$ mm, $s_c = 0.24$ mm, $w_v =$ 0.47 mm, $\ell_c = 20.5$ mm
$C_{ap} = 0.3$ pF $\rightarrow$ 135 Ω-6° long and 40 Ω-6.5° long

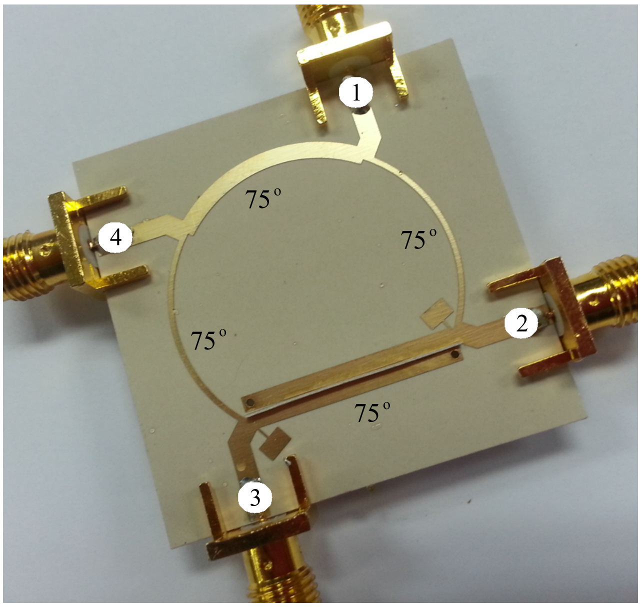

FIGURE 9. Fabricated prototype II (GCRHC) for $k^2 = -5$ dB.

The bandwidth with 15-dB return loss of $|S_{11}|$ is about 82.9 % (1.62-3.278 GHz), and that with 15-dB isolation is more than 150 %. The measured power divisions in Fig. 8(b) are $|S_{21}| = -3.33$ dB and $|S_{41}| = -3.08$ dB at 2 GHz. The measured phase responses of $\angle S_{21} - \angle S_{41}$ and $\angle S_{23} - \angle S_{43}$ in Fig. 8(c) are 1.617° and 181.36° at 2 GHz. Good agreements between measured and predicted results are achieved.

B. PROTOTYPE II FOR $k^2 = -5$ dB

For $k^2 = -5$ dB, the GCRHC topology was chosen, and the design parameters with $C = -5$ dB in Table 4 were applied.

The design and fabrication parameters are collected in Table 6 where $Z_1 = 98.83\ \Omega$, $Z_2 = 55.58\ \Omega$. $\Theta_1 = \Theta_2 = \Theta_3 = 75°$, $Z_{0e} = 71.41\ \Omega$, $Z_{0o} = 20\ \Omega$ and $C_{ap} = 0.3$ pF at 2 GHz. The value of $C_{ap} = 0.3$ pF should be half of that in Table 4, because the design frequency is modified from 1 GHz to 2 GHz.

The physical dimensions for the two different TLs are $w_1 = 0.51$ mm, $l_1 = 20.89$ mm, $w_2 = 1.61$ mm and $l_2 = 20.17$ mm where w_1 and l_1 are width and length of the 98.83- Ω TL, while those of w_2 and l_2 are for the 55.58- Ω TL. For the CPL, the coupling coefficient of C is -5 dB, and therefore 3D structure is needed. First consider $Z_{0e} = 71.41\ \Omega$ and $Z_{0o} = 42.5\ \Omega$ whose dimensions are $w_c = 1.45$ mm and the space $s_c = 0.24$ mm where only Z_{0e} is the required value for the measurements and $Z_{0o} = 42.5\ \Omega$ is not the required one but was chosen to fix at $s_c = 0.24$ mm. In this case, additional odd-mode impedance of 37.79 Ω is demanded so that the parallel connection of 37.79 and 42.5 Ω can be 20 Ω. Similarly, the width w_v of the vertical conductor can be obtained. For the 0.3 pF at 2 GHz, an open-circuited stepped impedance TL (135 Ω − 6° long and 40 Ω − 6.5° long) like the form in [7, Fig. 13(b)] was employed. The fabricated prototype II for $k^2 = -5$ dB is illustrated in Fig. 9.

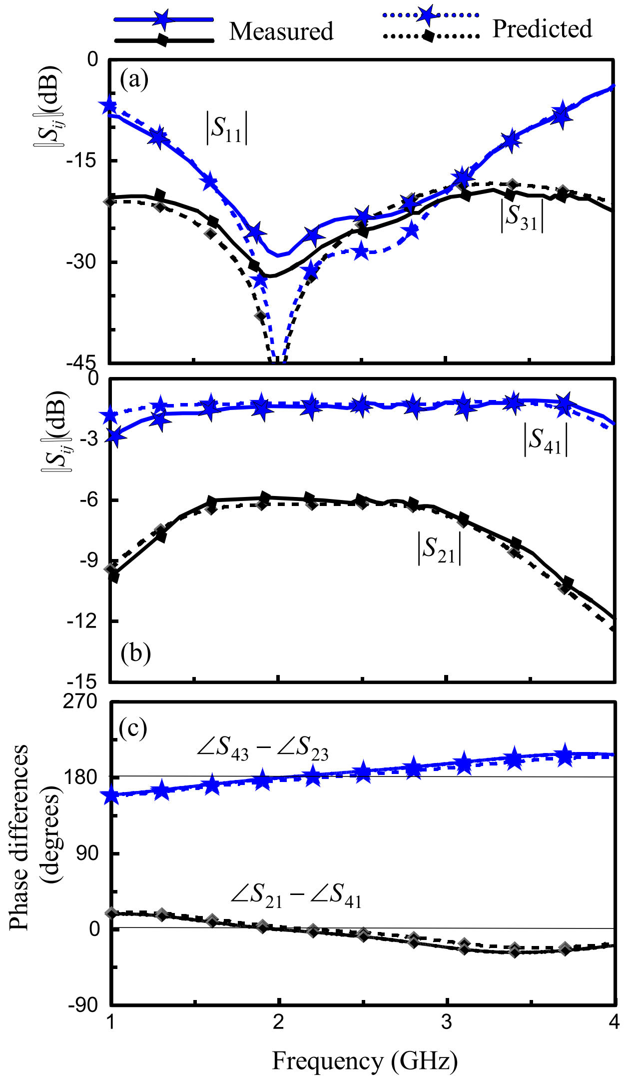

FIGURE 10. Measured and predicted frequency responses of prototype II (GCRHC) for $k^2 = -5$ dB. (a) $|S_{11}|$ (matching) and $|S_{31}|$ (isolation). (b) Power divisions of $|S_{21}|$ and $|S_{41}|$. (c) In- and out-of-phase responses.

The frequency responses measured and predicted are compared in Fig. 10 where matching at port ① and isolation frequency responses are in Fig. 10(a), while the power divisions in Fig. 10(b) and phase responses in Fig. 10(c). The measured

$|S_{11}|$ and $|S_{31}|$ in Fig. 10(a) are -29.18 and -32.36 dB at 2 GHz, respectively. The bandwidth with 15-dB return loss of $|S_{11}|$ is about 97.65 % (1.47-3.43 GHz) and the 15-dB isolation is achieved in whole frequencies of interest. The measured power divisions in Fig. 10(b) are $|S_{21}| = -6.25$ dB and $|S_{41}| = -1.12$ dB at 2 GHz. The measured phase responses of $\angle S_{21} - \angle S_{41}$ and $\angle S_{23} - \angle S_{43}$ in Fig. 10(c) are 0.891° and 180.28° at 2 GHz. Good agreements between measured and predicted results are also obtained.

V. CONCLUSIONS

In this paper, the GCRHs were presented to overcome the conventional disadvantages. Each consists three TLs and one CPL with or without capacitances. Two of the TLs are identical to each other, the rest TL and CPL are different from each other, which are of arbitrary electrical lengths less than or equal to 90° long. When all the TLs are 90° long, since two poles are located at the design frequency, perfect matching can be achieved only at the design frequency. However, as the electrical length starts to be less than 90°, perfect matching and pseudo matching can be achieved at two different frequencies, and the two frequency distance becomes wider with the electrical length smaller, which contributes to wider return loss bandwidths. Therefore, the fact that the electrical lengths of the GCRHs are less than 90°, is the advantage over the conventional ones, together with size reduction and wider bandwidths. Due to the fundamental advantages of the GCRHs and GCRHCs, diverse applications may be expected including wideband and compact RHs for arbitrary termination impedances.

REFERENCES

[1] W. A. Tyrrell, "Hybrid circuits for microwaves," *Proc. IRE.*, vol. 35, no. 11, pp. 1294–1306, Nov. 1947.
[2] S. March, "A wideband stripline hybrid ring," *IEEE Trans. Microw. Theory Techn.*, vol. MTT-16, no. 6, pp. 361–362, Jun. 1968.
[3] H. Ahn, I.-S. Chang, and S.-W. Yun, "Miniaturized 3-dB ring hybrid terminated by arbitrary impedances," *IEEE Trans. Microw. Theory Techn.*, vol. 42, no. 12, pp. 2216–2221, Dec. 1994.
[4] P.-J. Chou, C.-C. Yang, and C.-Y. Chang, "Exact synthesis of unequal power division filtering rat-race ring couplers," *IEEE Trans. Microw. Theory Techn.*, vol. 66, no. 7, pp. 3277–3287, Jul. 2018.
[5] S. Gruszczynski and K. Wincza, "Broadband rat-race couplers with coupled-line section and impedance transformers," *IEEE Microw. Wireless Compon. Lett.*, vol. 22, no. 1, pp. 22–24, Jan. 2012.
[6] H. R. Ahn and B. Kim, "Small wideband coupled-line ring hybrids with no restriction on coupling power," *IEEE Trans. Microw. Theory Techn.*, vol. 57, no. 7, pp. 1806–1817, Jul. 2009.
[7] H.-R. Ahn and S. Nam, "Compact microstrip 3-dB coupled-line ring and branch-line hybrids with new symmetric equivalent circuits," *IEEE Trans. Microw. Theory Techn.*, vol. 61, no. 3, pp. 1067–1078, Mar. 2013.
[8] H.-R. Ahn and S. Nam, "Wideband microstrip coupled-line ring hybrids for high power-division ratios," *IEEE Trans. Microw. Theory Techn.*, vol. 61, no. 5, pp. 1768–1780, May 2013.
[9] H.-R. Ahn and M. M. Tentzeris, "A novel wideband compact microstrip coupled-line ring hybrid for arbitrarily high power-division ratios," *IEEE Trans. Circuits Syst. II, Exp. Briefs*, vol. 64, no. 6, pp. 630–634, Jun. 2017.
[10] H.-R. Ahn, I. Wolff, and I.-S. Chang, "Arbitrary termination impedances, arbitrary power division, and small-sized ring hybrids," *IEEE Trans. Microw. Theory Techn.*, vol. 45, no. 12, pp. 2241–2247, Dec. 1997.
[11] L.-S. Wu, J. Mao, and W.-Y. Yin, "Miniaturization of rat-race coupler with dual-band arbitrary power divisions based on stepped-impedance double-sided parallel-strip line," *IEEE Trans. Compon., Packag., Manuf. Technol.*, vol. 2, no. 12, pp. 2017–2030, Dec. 2012.
[12] M.-H. Murgulescu, E. Moisan, P. Legaud, E. Penard, and I. Zaquine, "New wideband, 0.67 λ_g circumference 180o hybrid ring coupler," *Electron. Lett.*, vol. 30, no. 4, pp. 299–300, Feb. 1994.
[13] T. Wang and K. Wu, "Size-reduction and band-broadening design technique of uniplanar hybrid ring coupler using phase inverter for M(H)MIC's," *IEEE Trans. Microw. Theory Techn.*, vol. 47, no. 2, pp. 198–206, Feb. 1999.
[14] J. Rathore, S. Aditya, and S. C. D. Roy, "A general analysis and new designs for the hybrid-ring directional coupler," *Indian J. Technol.*, vol. 31, pp. 827–830, Dec. 1993.
[15] V. Napijalo, "Coupled line 180° hybrids with lange couplers," *IEEE Trans. Microw. Theory Techn.*, vol. 60, no. 12, pp. 3674–3980, Dec. 2012.
[16] C. Y. Pon, "Hybrid-ring directional coupler for arbitrary power divisions," *IRE Trans. Microw. Theory Techn.*, vol. 9, no. 6, pp. 529–535, Nov. 1961.
[17] H.-R. Ahn, *Asymmetric Passive Components in Microwave Integrated Circuits*. New York, NY, USA: Wiley, 2006.
[18] H.-R. Ahn, "Reply to 'Comments on reply to comments on 'Wideband coupled-line filters with high-impedance short-circuited stubs,''" *IEEE Microw. Wireless Compon. Lett.*, vol. 24, no. 5, pp. 357–359, May 2014.
[19] H.-R. Ahn and M. M. Tentzeris, "In-phase T-junction: Study and application to Gysel power dividers for high power-division ratios requiring no high-impedance transmission-line section," *IEEE Access*, vol. 7, pp. 18146–18154, 2019.
[20] H.-R. Ahn and M. M. Tentzeris, "Novel generic asymmetric and symmetric equivalent circuits of 90° coupled transmission-line sections applicable to marchand baluns," *IEEE Trans. Microw. Theory Techn.*, vol. 65, no. 3, pp. 746–760, Mar. 2017.

HEE-RAN AHN (S'90–M'95–SM'99) received the B.S., M.S., and Ph.D. degrees in electronic engineering from Sogang University, Seoul, South Korea.

From 1996 to 2002, she was with the Department of Electrical Engineering, Duisburg-Essen University, Duisburg, Germany, where she was involved with the Habilitation dealing in asymmetric passive components in microwave integrated circuits. From 2003 to 2005, she was with the Department of Electrical Engineering and Computer Science, Korea Advanced Institute of Science and Technology, Daejeon, South Korea. From 2005 to 2009, she was with the Department of Electronics and Electrical Engineering, Pohang University of Science and Technology, Pohang, South Korea. From 2009 to 2010, she was with the Department of Electrical Engineering, University of California at Los Angeles, Los Angeles, CA, USA. From 2011 to 2014, she was with the School of Electrical Engineering and Computer Science, Seoul National University, Seoul, South Korea. Since 2015, she has been with the School of Electrical and Computer Engineering, Georgia Institute of Technology, Atlanta, GA, USA, as a Visiting Scholar. She has authored the book *Asymmetric Passive Component in Microwave Integrated Circuits* (Wiley, 2006). Her current research interests include high-frequency and microwave circuit designs, and biomedical applications using microwave theory and techniques.

MANOS M. TENTZERIS (M'98–SM'03–F'10) received the Diploma degree *(magna cum laude)* in electrical and computer engineering from the National Technical University of Athens, Greece, and the M.S. and Ph.D. degrees in electrical engineering and computer science from the University of Michigan, Ann Arbor, MI, USA. He was a Visiting Professor with the Technical University of Munich, Germany, in 2002, GTRI-Ireland, Athlone, Ireland, in 2009, and LAAS-CNRS, Toulouse, France, in 2010. He is currently the Ken Byers Professor in flexible electronics with the School of ECE, Georgia Institute of Technology (Georgia Tech), Atlanta, GA, USA. He also heads the ATHENA Research Group (20 researchers). He has helped to develop academic programs in 3-D/inkjet-printed RF electronics and modules, flexible electronics, origami and morphing electromagnetics, highly integrated/multilayer packaging for RF and wireless applications using ceramic and organic flexible materials, paper-based RFIDs and sensors, wireless sensors and biosensors, wearable electronics, "green" electronics, energy harvesting and wireless power transfer, nanotechnology applications in RF, microwave MEMs, SOP-integrated (UWB, multiband, mmWave, and conformal) antennas. He has served as the Head of the GT-ECE Electromagnetics Technical Interest Group, as the Georgia Electronic Design Center Associate Director for RFID/Sensors Research, as the Georgia Tech NSF-Packaging Research Center Associate Director for RF Research, and as the RF Alliance Leader. He has authored over 700 papers in refereed journals and conference proceedings, five books, and 25 book chapters. He is a member of the URSI-Commission D, the MTT-15 Committee, and the Technical Chamber of Greece, an Associate Member of the EuMA, and a Fellow of the Electromagnetic Academy. He was a recipient/co-recipient of the 2015 IET Microwaves, Antennas and Propagation Premium Award, the 2014 Georgia Tech ECE Distinguished Faculty Achievement Award, the 2014 IEEE RFID-TA Best Student Paper Award, the 2013 *IET Microwaves, Antennas and Propagation*Premium Award, the 2012 FiDiPro Award in Finland, the iCMG Architecture Award of Excellence, the 2010 IEEE Antennas and Propagation Society Piergiorgio L. E. Uslenghi Letters Prize Paper Award, the 2011 International Workshop on Structural Health Monitoring Best Student Paper Award, the 2010 Georgia Tech Senior Faculty Outstanding Undergraduate Research Mentor Award, the 2009 IEEE TRANSACTIONS ON COMPONENTS AND PACKAGING TECHNOLOGIES Best Paper Award, the 2009 E. T. S. Walton Award from the Irish Science Foundation, the 2007 IEEE APS Symposium Best Student Paper Award, the 2007 IEEE IMS Third Best Student Paper Award, the 2007 ISAP 2007 Poster Presentation Award, the 2006 IEEE MTT Outstanding Young Engineer Award, the 2006 Asian–Pacific Microwave Conference Award, the 2004 IEEE TRANSACTIONS ON ADVANCED PACKAGING Commendable Paper Award, the 2003 NASA Godfrey Art Anzic Collaborative Distinguished Publication Award, the 2003 IBC International Educator of the Year Award, the 2003 IEEE CPMT Outstanding Young Engineer Award, the 2002 International Conference on Microwave and Millimeter-Wave Technology Best Paper Award in Beijing, China, the 2002 Georgia Tech-ECE Outstanding Junior Faculty Award, the 2001 ACES Conference Best Paper Award, and the 2000 NSF CAREER Award and the 1997 Best Paper Award of the International Hybrid Microelectronics and Packaging Society. He was the TPC Chair of the IEEE IMS 2008 Symposium and the Chair of the 2005 IEEE CEM-TD Workshop. He is the Vice-Chair of the RF Technical Committee (TC16) of the IEEE CPMT Society. He is the Founder and the Chair of the RFID Technical Committee (TC24) of the IEEE MTT Society and the Secretary/Treasurer of the IEEE C-RFID. He is an Associate Editor of the IEEE TRANSACTIONS ON MICROWAVE THEORY AND TECHNIQUES, the IEEE TRANSACTIONS ON ADVANCED PACKAGING, and the *International Journal on Antennas and Propagation*. He has given more than 100 invited talks to various universities and companies all over the world. He served as one of the IEEE MTT-S Distinguished Microwave Lecturers, from 2010 to 2012, and he is one of the IEEE CRFID Distinguished Lecturers.